Influence of freezing directions on ice lens formations in soils

K. Niggemann*[1], M. Ziegler[2], R. Fuentes[1]

[1] Institute of Geomechanics and Underground Technology, RWTH Aachen University, Germany. Email: [niggemann, raul.fuentes]@gut.rwth-aachen.de,

[2] Ziegler und Aulbach Ingenieurgesellschaft GmbH (formerly RWTH Aachen University, Germany). Email: ziegler@zai-ingenieure.de

* Corresponding author

Abstract. This research work presents a comprehensive experimental study of frost heave in a fine-grained material to investigate the effects of top freezing (TF) and bottom freezing (BF) mechanisms with ice lens formation. A novel test device was built to investigate artificial ground freezing (AGF) -related temperature and load boundary conditions. This paper includes 62 frost heave experiments and test observations up to 10 days. The long test duration allows a precise examination of ice lens growth during thermal steady state when the frost line remains largely stable and the ice lens grows. This state corresponds to the holding phase of a practical in-situ AGF implementation where the cooling is used to maintain the frozen body thickness. The freezing observations show that BF heaving is larger than TF heaving in most cases. This is caused by the more favourable hydraulic conditions caused by gravitational effects and vertical cracking that occurs during ice lens formation due to suction. This facilitates water accumulation at the ice lens. An applied load reduces the differences between BF and TF conditions beyond a certain value which corresponds to an overburden capable of preventing the formation of the longitudinal cracks.

Keywords: Top freezing; bottom freezing; frost heave; ice lenses; artificial ground freezing; experimental study

1 Introduction

The method of artificial ground freezing (AGF) was adapted to Civil Engineering works from the mining industry, after the engineer Herman Poetsch invented it in 1883 [1]. The application of AGF to support unstable soils and systems became a very popular method in the last decades, especially for the development of underground infrastructure in inner-city areas. It is an efficient method with a double temporary soil supporting and waterproofing function. However, freezing is also associated to frost induced soil deformations and frost heave that can cause damage to pipelines, pavements as well as foundations and buildings. The pore water volume expands by 9 % approximately during freezing [2]. Depending on the saturation degree and the hydraulic conductivity, a part of the water can be drained off during freezing. However, in more frost sensitive soils, like silt or clay, the water cannot be expelled during rapid cooling and freezes in situ due to their small hydraulic conductivity. Moreover, pure ice layers (ice lenses) can form in these fine-grained soils which can grow to several centimeters in height depending on the boundary conditions. As water is, by definition, available in soils where AGF is applied, this source of water supports ice lens formation.

These lenses develop in a semi-frozen area (frozen fringe), between the unfrozen and frozen soil, that contains ice as well as unfrozen water at sub-zero temperatures. In the frozen fringe, liquid water films form around grains and this drives the water migration (e.g. [3-6]) due to suction [7]. The thickness of the ice lenses depends on the soil type, water availability, freezing temperatures, speed of freezing (frost penetration rate) and overburden load. With decreasing permeability due to sub-zero temperatures, the water flow is stopped, and water accumulation occurs on another level in the frozen fringe, where another ice lens could form. When the frost no longer penetrates, the largest and thus, in terms of total heave, most significant ice lens, is formed. Since there are still thermal processes occurring during ice lens formation, this phase is also called quasi-steady state [8].

AGF and natural soil freezing in fine material present similar soil freezing mechanisms, including the formation of ice lenses. However, the different boundary conditions present in both scenarios on the total heave and ice lens formation have not been fully presented to date. The freezing direction is of interest and shows different characteristics as explained in the next section and observed from the literature presented in Table 1. In AGF, freezing occurs in multiple directions (e.g., tunnel cross section), where the largest surface heave occurs due to upwards freezing (Fig. 1) using brine at temperatures of ≈ -35°C [9]. Considering seasonally soil freezing in

natural conditions, the frost penetrates the soil from the top downwards due to sub-zero temperatures, a condition that may also apply to AGF, but usually at temperatures above -15°C [10]. The different temperatures are important as larger temperature gradients are known to reduce ice lens formation during frost penetration.

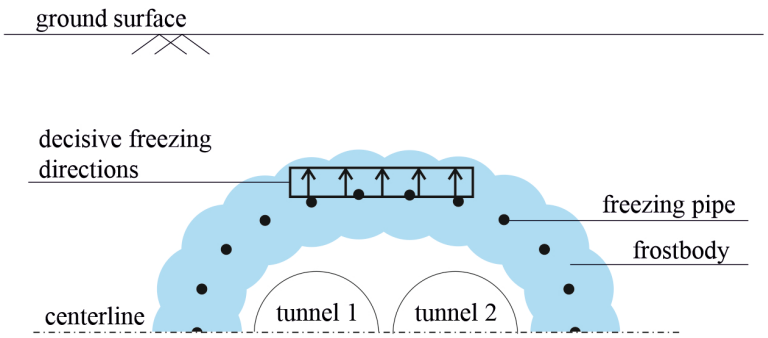

Fig. 1 Freezing directions at AGF of a tunnel cross section

At natural freezing, the investigations focus on frost heave during ongoing frost penetration. In that case the frost line, where ice lenses form, is a moving boundary and the ice lens formation is restricted by the freezing velocity. An apparently infinite ice lens can form when the frost line maintains at a specific position due to thermal (quasi-) equilibrium (there are still thermal processes due to ice lens formation, but of minor interest concerning frost penetration). This quasi-steady state is comparable with the holding phase at AGF, where the thickness of the frozen body is only preserved but over a longer time period. Assuming infinite ice lens growth, the quasi-steady state at the AGF is the governing state to be considered.

In the last decades many frost heave tests were carried out by several researchers who investigated the frost sensitivity of different soils as well as the influences of freezing temperatures and/or loads on frost heave, e.g., [8, 11-16]. Table 1 summarizes the test conditions. The dimensions of the test cylinders vary in height h between 7 cm and 25 cm and in diameter d between 3.7 cm and 14.6 cm. Kaplar [11] used a conical test cylinder to reduce friction between the specimen and the cylinder during frost heaving. Others have used freezing conditions from the bottom upwards to reduce friction (bottom freezing).

Table 1 Frost heave test conditions from the literature

	specimen size [cm]	soil type	freezing direction	freezing temperature/-conditions	load [kPa]
Kaplar [11]	h = 15.2 d_{top} = 14.6 d_{bottom} = 14.0	gravelly silty sand	TF	near 0°C; frost penetration: 0.6-1.3 cm/d	3.4
Penner and Ueda [12]	h = 10.2 d = 10.2	silty sand, sandy silt, clayey silt	BF	up to -2°C	consol.: 392-490 freezing test: 49-490
Loch and Kay [17]	h = 7.0-7.4 d = 3.7	New Hampshire Silt	BF	up to -7°C	7.7-65.2
Konrad and Morgenstern [8]	h = 25.0 d = 10.0	Devon Silt	TF	-2.5 to -6.2°C	consol.: 210 freezing test: -
Konrad and Morgenstern [15]			TF	-3.5 to -6.0°C	
Konrad and Morgenstern [16]			BF	$gradT_f$ = 0.63-1.11°C/cm	consol.: 210 freezing test: 45-400
Jin et al. [14]	h = 10.0 d = 10.0	Joomunjin Sand and Kaolinite, weathered granite	BF	-8 to -9.5°C	1.62

Hence, multi-direction freezing tests exist and the literature shows there are differences between TF and BF concerning the freezing, expansion, and water flow direction, which influences consolidation processes as well as water accumulation during ice lens formation. However, a systematic study to investigate the effect of different freezing directions on ice lens heave by direct comparison of heaving under identical thermal or load conditions is not available. In this work, heave differences are quantified in terms of AGF-related boundaries concerning thermal and load conditions. We carried out 62 frost heave experiments in a novel frost heave apparatus that can perform TF and BF tests to ensure identical boundary conditions. The test duration of about 10 days provides sufficient opportunity to observe the thermal steady state in which the largest ice lens is formed.

For this purpose, the new test device for the TF and BF tests is explained in section 2. Section 3 and 4 provide information on the test material and the testing program. The following sections 5 and 6 focus on the test evaluation and the test results. Finally, the results are briefly summarized and conclusions are given.

2 Experimental design and description

The new experimental setup is shown in Fig. 2. The dimensions of the cylindrical specimen are 25 cm in diameter and 20 cm in height. The test cylinder consists of eight PVC ring elements, with a thickness of 2.5 cm, connected by a tongue and groove system to prevent lateral displacement. The ring elements lying on top of each other were sealed by a rubber ring so that no water leaks out of the unfrozen soil. For specimen installation, the rings were additionally screwed together. During the freezing test, the ring elements can be pulled and move apart vertically, so that the soil samples do not undergo any frictional resistance due to the vertical expansion. The top and the bottom of the samples, respectively, were cooled by a freezing element (1) which is connected to a cooling circulation thermostat (CC-508, Huber Kaeltemaschinenbau AG, Germany). The freezing temperature was controlled by a temperature sensor placed in the freezing element. As refrigerant, a silicone oil that can be cooled down to -60°C (Thermofluid M60.115/200.05, Huber Kaeltemaschinenbau AG, Germany) was used. A water reservoir (6) was connected to a filter plate (2) at the warm side of the sample, providing a constant water supply under atmospheric pressure for ice lens formation. The diameter of the reservoir was chosen to be very large with 29 cm, to provide sufficient water availability for ice lens formation, but with a very low water head of approximately 1 cm. In the BF tests, the position of the water reservoir placed at the top of the sample was adjusted during the freezing test to compensate for the vertical specimen expansion. The warm end of the soil sample was additionally heated by a heating plate (3) that is connected to a warming circulation thermostat (Kiss 104A, Huber Kaeltemaschinenbau AG, Germany) to avoid freezing of the overall sample. Water was used as circulating fluid for heating process. The test cylinders were covered with a Styrodur insulation (BASF, Germany). All tests were carried out in a climatic chamber with a constant temperature of 15°C (initial temperature of the soil before freezing) and humidity of 40 % to exclude influences such as seasonal fluctuations.

For the experimental study without considering overburden pressure (Fig. 2a), a load results only from the apparatus elements (i.e., the porous heating plate for BF and the freezing plate for TF) and an additional static

10 kg load to ensure a frictional connection between the plates and the sample. This results in a total load of p = 3.6 kPa.

The test series considering overburden load (Fig. 2b) were carried out using a drive (7) (Spindeltrieb 10 kN + SMS 94, Pero, Germany) to apply loads between 50 kPa and 250 kPa to the sample from the top. The load was applied using a cylinder connected to an electric spindle. The loading was deformation-controlled with a rate of 0.5 mm/min until the required load was applied. Subsequently, the load was kept constant during consolidation and freezing phase. The automatic load control was performed every 60 seconds. After consolidation, the soil has settled in the test cylinder. Using an adapter (steel plate) (8) that was installed between the soil and the freezing element from the beginning, heat transfer from the freezing element into the soil by conduction was ensured during the whole test procedure (the freezing element cannot enter the test cylinder due to connections). To achieve the same heat transfer through the adapter, the thickness of the adapter (1 cm) was set equal in all load tests depending on the pre-tested settlement after maximum loading with 250 kPa.

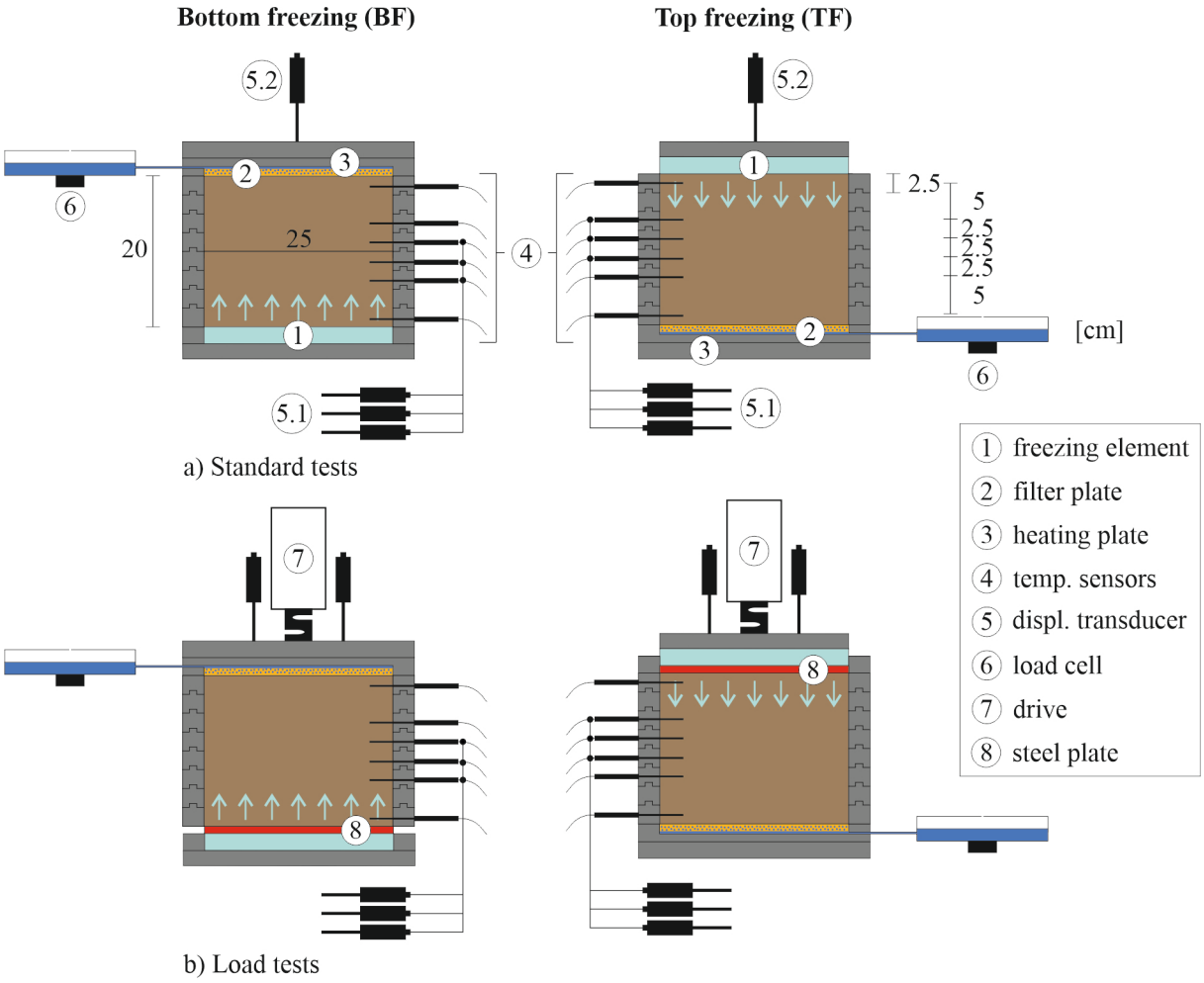

Fig. 2 Test setup for TF and BF, for a) standard tests and b) load tests

2.1 Instrumentation

For data recording, temperature sensors (MWT1/10, TMH GmbH, Germany) (4) were distributed over the sample height, see Fig. 2. After consolidation, the temperature sensors were placed into the soil sample through small openings in the ring elements. During frost heaving the sensors move together with the ring elements. The vertical deformation was measured by displacement transducers (LRW2-C-50, WayCon Positionsmesstechnik GmbH, Germany) that are connected to the temperature sensors (5.1). The displacement transducers were attached to the ring elements that move vertically during the freezing process. For the data recording of the total uniaxial deformation at the top of the specimen the same type of displacement transducer (LRW2-C-50, WayCon Positionsmesstechnik GmbH, Germany) were used (5.2). This temperature and displacement monitoring allows

the calculation of the freezing front velocity which is important to distinguish between the thermal transient and steady state (cf. section 5.3). To determine the water inflow into the sample due to suction, the mass of the water supply was recorded by a load cell (S2, HBM, Austria) (6). The load of the drive was controlled by a connected load cell (KDB, Pero, Germany) (7).

3 Test material and preparation

The test material was produced artificially to ensure an equal composition for all tests and, thus, to improve the repeatability and consistency of the results. With a liquid limit (LL) of 32.9 % and a plasticity index (PI) of 14.5 % the soil can be classified as a lean clay (CL, Unified Soil Classification System). The grain size distribution can be found in [18]. The dry material was prepared with a mass water content of 20 % to ensure a high saturation as well as an appropriate consistency, and subsequently stored for 24 hours to ensure that the water can penetrate into the pores. Afterwards the water content of the soil was proved for each test by a drying procedure. The values of the mean water content $\bar{x}_w$ and saturation $\bar{x}_{Sr}$, and standard deviation σ_w and σ_{Sr} for the 32 TF and 30 BF tests, presented in Table 2, confirm the good repeatability of the process.

Table 2 Mean value $\bar{x}$ and standard deviation σ of water content w and saturation S_r for TF and BF

	n [−]	$\bar{x}_w$ [%]	σ_w [%]	$\bar{x}_{Sr}$ [%]	σ_{Sr} [%]
TF	32	20.37	0.55	91.70	2.60
BF	30	20.33	0.60	91.30	2.73

The hydraulic conductivity of the soil was tested several times with the same initial conditions of porosity and saturation degree as the test specimen. The mean value is $1.3 \cdot 10^{-10}$ m/s ($\sigma_k = 5.3 \cdot 10^{-11}$ m/s) or $1.8 \cdot 10^{-17}$ m^2 ($\sigma_K = 7.0 \cdot 10^{-18}$ m^2). The soil was compacted in eight layers in the test cylinder by 40 blows with a 4.5 kg proctor hammer. The mean moist density achieved is 2.022 g/cm^3 ($\sigma_\rho = 0.017$ g/cm^3).

The prepared soil in the test cell was stored for approx. 24 hours in the climatic chamber at 15°C to ensure a uniform material temperature at the beginning of each test. The material temperature was monitored by the temperature sensors already installed. After acclimatization, when all sensors reached 15°C, the freezing process started. Simultaneously, the tempering process began on the warm side of the specimen. Depending on the thermal boundary conditions, one freezing test took up to 2 days to reach thermal quasi-steady state conditions. Afterwards the test ran about 8 more days to provide a long thermal steady state phase.

4 **Testing program**

The main task of the experimental program is the observation of TF vs. BF under variation of the following parameters:

- absolute freezing temperature T_f
- temperature gradient in the frozen area $gradT_f$
- external load p

Additionally, a test was carried out with *restricted water supply* W_{ws0} at a freezing temperature of T_f = -10°C to study the effect of no additional available water.

Table 3 summarizes the main values of the tests. The parameter $T_{c,ts}$ describes the recorded cold side temperature during steady state conditions measured by the nearest temperature sensor to the cold edge (cf. Fig. 2). Similarly, $T_{w,ts}$ describes the measured temperature on the warm side. The values for n_{TF} and n_{BF} correspond to the number of experiments for one parameter variation. Where more than one test was performed, the figures are mean values for that single parameter combination.

Table 3 Main values of the experimental parameter study

tested parameter	T_f $[°C]$	$T_{c,ts}$ $[°C]$	$T_{w,ts}$ $[°C]$	W_{ws} [%]	$gradT_f$ $[°C/cm]$	p $[kPa]$	n_{TF} $[-]$	n_{BF} $[-]$
T_f $[°C]$	-5	-4.3	10.4	100	1.0	0	3	3
	-7.5	-6.9	8.6				2	2
	-10	-9.0	8.0				6	4
	-12.5	-11.3	6.9				1	1
	-15	-13.9	5.4				4	4
	-17.5	-16.0	4.6				1	1
W_{ws0} $[-]$	-10	-9.2	6.9	0	1.0	0	1	1
$gradT_f$ $[°C]$	-15	-13.5	13.6	100	1.5	0	3	3
	-7	-6.5	5.2		0.8		3	3
p^* $[kPa]$	-12.5	-12.2	6.0	100	1.0	50	1	1
		-12.2	5.5			100	1	1
		-12.4†	5.2			150	1	1
		-12.4†	4.7			200	1	1
		-12.5†	5.0			250	1	1
	-5	-4.9	9.8			50	1	1
		-5.0†	9.2			250	1	1
	-10	-9.6†	6.7			250	1	1

* placement of temperature sensors after consolidation

† extrapolated values on cold side; due to consolidation the nearest cold side temperature sensor could not be placed

The *absolute freezing temperature* T_f controls the frost penetration as show in Fig. 3 for a BF test. Values of T_f between -5°C and -17.5°C were imposed using a temperature sensor placed in the freezing element as control. On the warm side the water is heated up to 25°C that prevents freezing of the whole sample (please note the actual

temperature of the warm side is lower than 25°C due to the higher cooling capacity in the system). The temperature gradients along the frozen or unfrozen soil remain constant after reaching thermal quasi-steady state conditions.

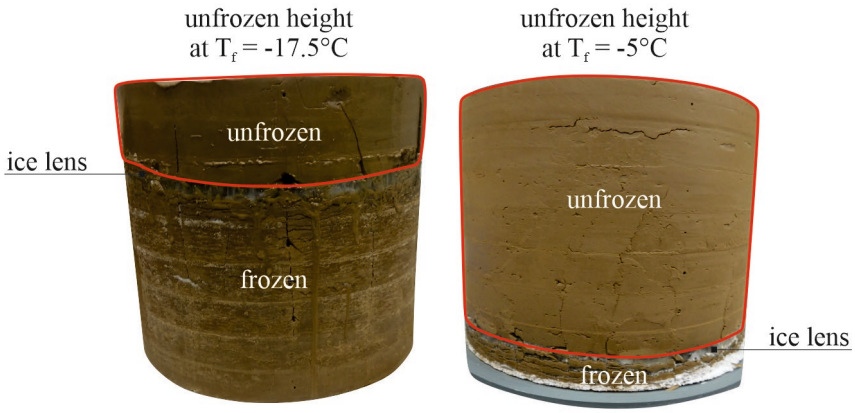

Fig. 3 Unfrozen soil part/flow path (red box) for a freezing temperature of -17.5°C (left) and -5°C (right), BF

To investigate the influence of different *temperature gradients* $gradT_f$ in the frozen area on frost heave and ice lens formation, the cold and warm side temperatures were adjusted to reach the same frost penetration depth (in the center of the sample) at different freezing and heating temperatures. The resulting temperature gradients are 0.8°C/cm, 1.0°C/cm and 1.5°C/cm (see Table 3).

For the tests with *external load* p, the soil samples were loaded between 50 kPa and 250 kPa, 50 kPa intervals, from the top of the sample, corresponding to overburdens of approximately 2.6 m, 5.3 m, 7.9 m, 10.5 m and 13.2 m ($\rho_{soil} \approx 1.9$ g/cm^3).

5 Evaluation of experimental tests

5.1 Sample examination at the end of the freezing test

After each test, the sample was removed from the test cylinder and visually observed. Subsequently the sample water content was determined in the longitudinal direction. For this purpose, the sample was divided into approx. 2.5 cm thick layers (the final ice lens thickness was between ≈0.5 cm and ≈1.5 cm) and dried for about 4 days at 105°C. The results provide details about the water distribution in the soil sample after freezing. Fig. 4 shows the water distribution at the end of BF with a freezing temperature of -10°C as an example (others are provided in the

Supplementary Material 1). With different freezing temperatures the position of the ice lens changes, but qualitatively the water distribution in the frozen and unfrozen part is very similar. In the frozen area the water content slightly increases due to minor ice lens formation during transient freezing. In the unfrozen area close to the last ice lens, which is built under quasi-steady state conditions, the water content decreases. It indicates that soil water was drained off the area near the ice lens without a direct flow from the reservoir water through suction [19].

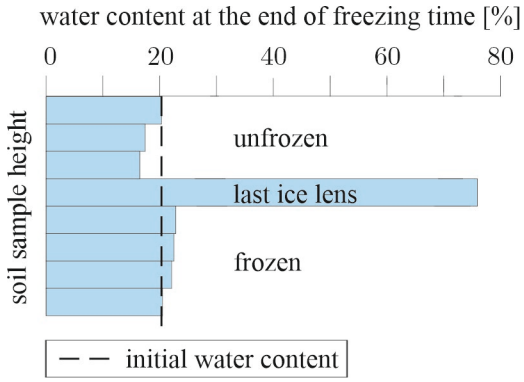

Fig. 4 Soil water distribution after freezing (T_f = -10°C) for BF

Fig. 5 shows the measured reservoir water mass that is sucked into the soil sample as a proportion of the total water mass that is used for the ice lens formation. The dashed line indicates the pore water mass used for ice lens formation, calculated as the difference between the measured sucked water from the reservoir and the total water mass for ice lens formation. The latter is calculated as the ice lens heave (heave measurement) divided by the expansion factor of 1.09 due to phase change. At the beginning of ice lens formation, most of the sucked water comes from water-filled soil pores, because the water from the external reservoir is initially saturating air-filled pores before reaching an unrestricted flow to the ice lens. With time, most water for ice lens formation comes from the reservoir. The lower the freezing temperature the shorter it takes for the water from the reservoir to reach the ice lens and become dominant.

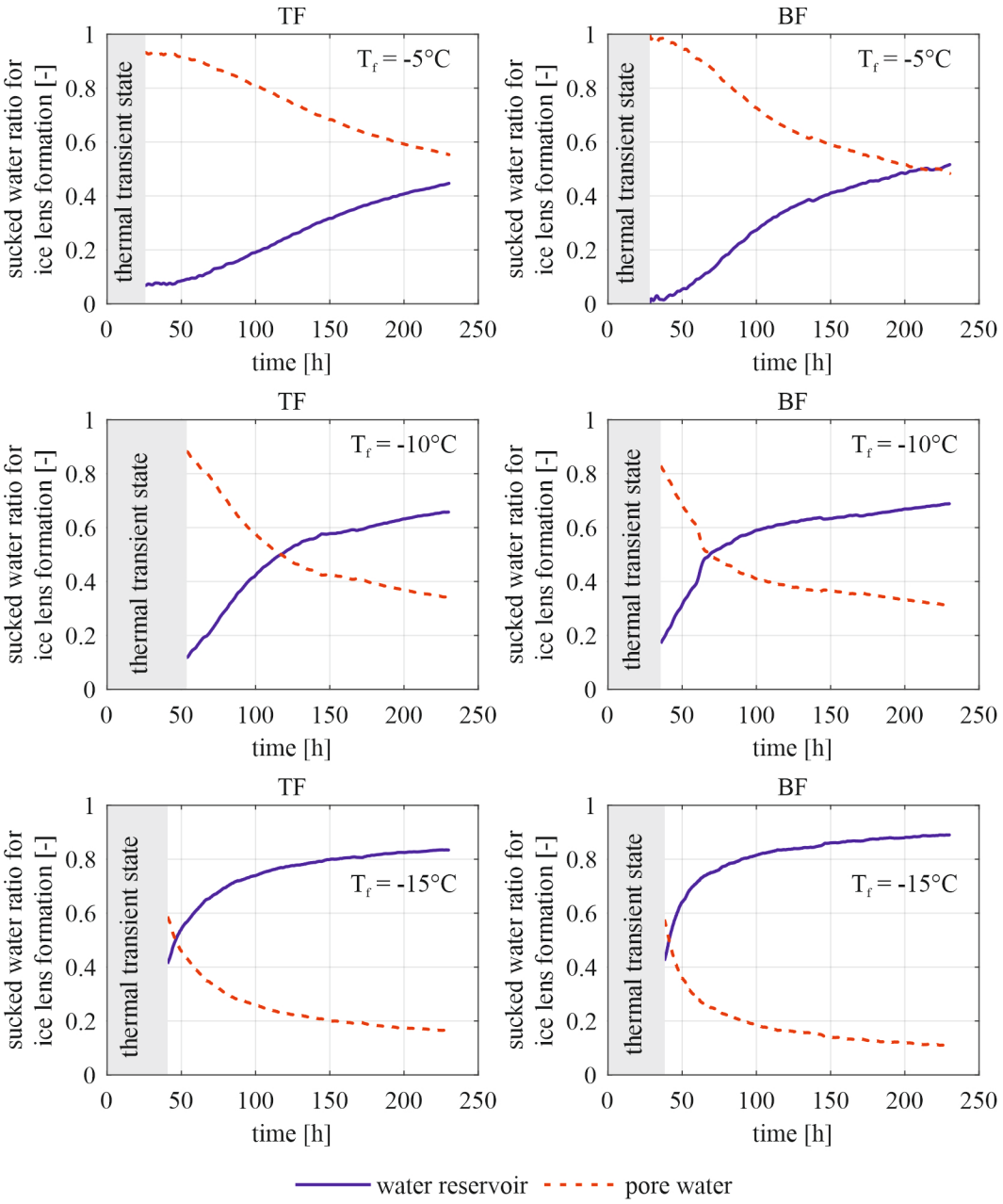

Fig. 5 Origin of the water for the formation of ice lenses at different freezing temperatures for TF and BF

After the freezing process, longitudinal cracks along the unfrozen sample height were investigated (Fig. 6a). They arise in the unfrozen area close to the ice lens and are a consequence of the reduced water content near the ice lens observed in Fig. 4. The unfrozen soil shrinks as water drains off for ice lens formation without sufficient water supply and a pattern cross section with openings is formed (Fig. 6b). This phenomenon of crack formation was

also observed by other scientists e.g., [20], [21] and [22] and it applies particularly to impermeable soils where greater suctions occur. The crack formation increases the water migration to the ice lens [18, 23-25].

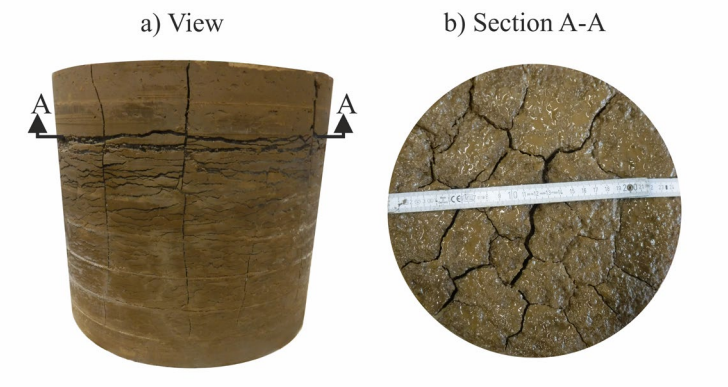

Fig. 6 Longitudinal crack formation of a BF sample

5.2 Evaluation of measured data

5.2.1. Determination of 0°C-isotherm

The recorded temperature and position over time for each temperature sensor are used to calculate the moving frost line, or 0°C-isotherm. This is important to calculate the temperature gradients in the frozen and unfrozen soil. The temperature distribution is also necessary for the definition of the thermal transient and quasi-steady states. Fig. 7 shows a calculated 0°C-isotherm position (a) and the corresponding frost penetration velocity v_{fp} (b). Fig. 7b allows differentiating between the two distinct stages. When reaching thermal quasi-steady state conditions, the frost penetration velocity approaches zero. The beginning of the thermal quasi-steady state is also defined by a critical frost penetration velocity $v_{fp,crit}$ less than 0.01 cm/h. From this point onwards only ice lens growth occurs, and shortly after, the frost penetration reaches a constant value. Similar graphs apply to other temperatures and are presented in the Supplementary Material 2.

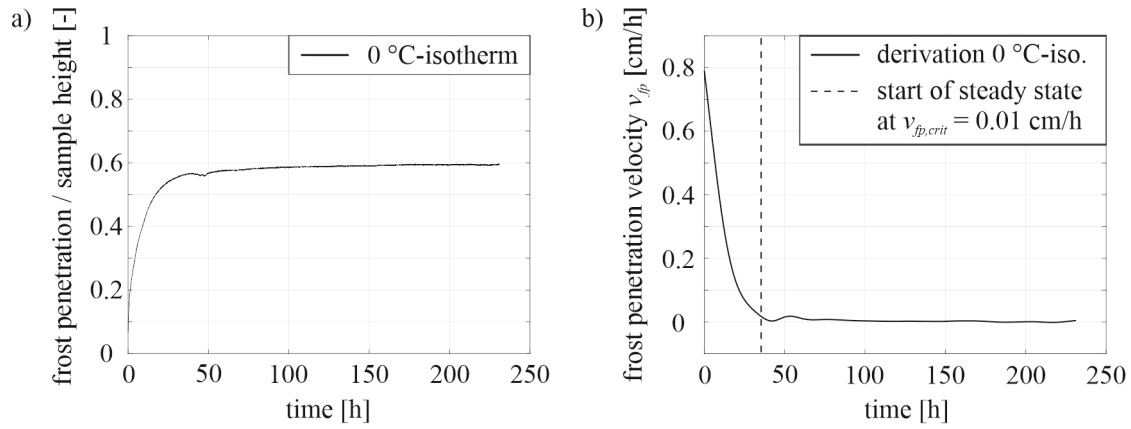

Fig. 7 a) Course of the 0°C-isotherm and b) corresponding frost penetration velocity for BF with a freezing temperature of -12.5°C

5.2.2. Determination of the heave proportions

Fig. 8 shows the results of frost heave at thermal transient and quasi-steady state for BF at a freezing temperature of -10°C. The total heave at thermal transient conditions is very low compared to the total heave at the thermal quasi-steady state, showing the importance of the thermal quasi-steady state for AGF. In the thermal transient state the pore water heave h_{PW} is determined by the one-dimensional pore water expansion of 9 % due to the frost penetration $x(t)$ using the porosity n and the saturation degree S_r as shown in equation 1. It is assumed that the water freezes at 0°C and does not expand in air filled voids.

$$h_{PW}(t) = 0{,}09 \cdot n \cdot S_r \cdot x(t) \tag{1}$$

The difference between total heave (h_{tot}) and pore water expansion (h_{PW}) is the calculated ice lens heave (h_{IL}). Consolidation effects are neglected because the load on the soil is very low at about 5 kPa, except for load tests. For thermal quasi-steady state, the ice lens heave is equal to the total heave.

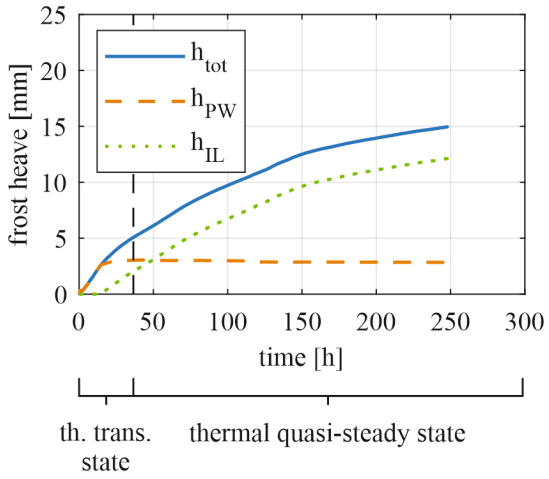

Fig. 8 Frost heave during thermal transient and quasi-steady state for a freezing temperature of -10°C, BF

6 **Test results**

The following subsections contain the frost heave results of 62 experiments according to the parameter variations explained in section 4 and summarized in Table 3.

6.1 Absolute freezing temperature T_f

The actual freezing temperature (T_f) determines the frost penetration depth and therefore the frozen and unfrozen soil height. The lower the freezing temperature the greater the frost penetration or frozen part of the soil at the thermal quasi-steady state. To compare the results during thermal transient freezing, with pore water expansion and minor ice lens formation, the frost heave is related to the frozen part. The relationship between frost heave and the height of the frozen part is proportional because all tests have similar values of volumetric porosity n and saturation degree S_r (cf. Table 2 and Equation 1 in subsection 5.2.2). Fig. 9 shows a similar curve for all tests. At TF the slope of the frost heave related to the frozen height is greater at the beginning, decreases with time and ends up in a straight line that indicates a constant rate of frost heave. At BF, the curve is like TF, except of a lower gradient at the beginning of freezing due to the overburden soil weight which decreases frost heaving.

Generally, ice lenses grow thicker (greater heave) at a decreasing frost penetration rate (i.e., higher freezing temperatures) because more time is available for water accumulation (refer also to Fig. 5).

Of particular interest is that most lines show a similar linear trend towards the end of this transient stage. Table 4 shows a straight line fit to the lines for this latter part, showing that for all temperatures with absolute temperature lower than -10°C, the frost heave increases at the same rate with time. This agrees with the fact that during this transient stage, the ice lens formation is minimal, and the frost heave is a consequence of porewater expansion, which depends on porosity and the amount of freezing water, which can be estimated as the position of the frost line. However, for higher temperatures, -5°C and -7.5°C, the heave grows faster relative to the frozen height indicating additional heaving by ice lenses.

The differences between BF and TF are related to the absolute values shown in Fig. 9 where BF shows generally lower values of heave. This shift is possibly due to the increased overburden in BF. Table 4 shows that the actual trends are generally very similar between BF and TF which indicates that, even at transient stage, the frost heave growth rate is governed by the temperature boundary conditions.

Furthermore, the heave result due to a restricted water supply (W_{ws0}) follows the other curves, showing that the restricted water supply does not have an impact on frost heave during transient freezing because of minor ice lens formation.

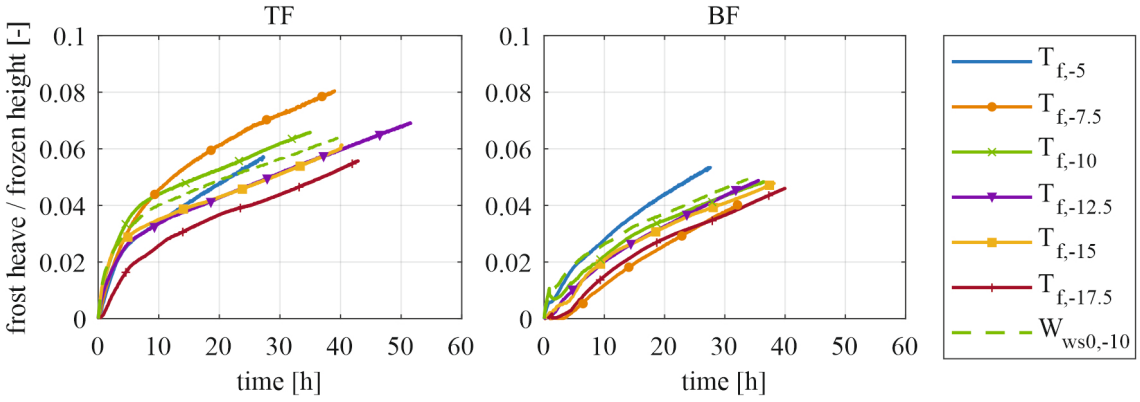

Fig. 9 Frost heave related to the frozen soil part at the thermal transient state for varied absolute freezing temperatures (T_f in °C) with (W_{ws0}) and without restricted water supply over time for TF and BF

Table 4 Linear heave slope for transient freezing

	(frost heave/frozen height)/time [1/h]	
	TF	BF
$\boldsymbol{T_{f,-5}}$	**0,00131**	**0,00139**
$\boldsymbol{T_{f,-7.5}}$	**0,00099**	**0,00118**
$T_{f,-10}$	0,00077	0,00083
$T_{f,-12.5}$	0,00083	0,00103
$T_{f,-15}$	0,00091	0,00087
$T_{f,-17.5}$	0,00084	0,00089
$W_{ws,-10}$	0,00075	0,00087

The heave at thermal quasi-steady state conditions results only from ice lens formation and is shown in Fig. 10. In general, the lower the temperature, the larger the ice lens heave is. The increasing frost penetration due to the lower temperature boundary condition decreases the flow path between ice lens and water reservoir. A shorter flow path enhances the water supply for ice lens formation due to an increasing water flow velocity from the water reservoir to the ice lens. Therefore, at thermal quasi-steady state conditions, the frost heave depends on the flow path (unfrozen soil height) and is not controlled by the height of the frozen part (cf. transient state). The frost heave rate due to a restricted water supply (W_{ws0}) strongly decreases over time as only the surrounding soil water can be used to form the ice lens. At this stage, it is therefore critical that water is available for heave to continue.

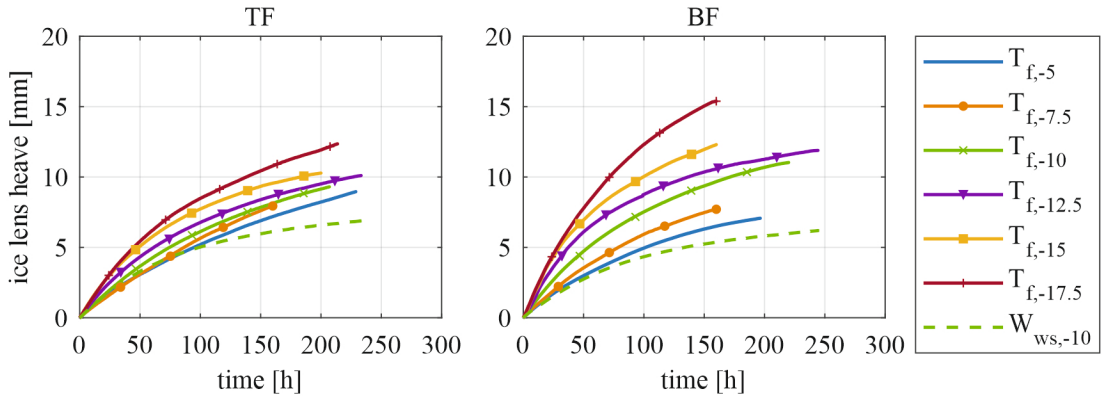

Fig. 10 Ice lens heave at the thermal quasi-steady state for different absolute freezing temperatures (T_f in °C) with (W_{ws0}) and without restricted water supply over time for TF and BF

Fig. 11 shows the dependency between frost heave due to ice lens formation and the length of the flow path (unfrozen height) 150 h after the beginning of quasi-steady state conditions. With decreasing flow path, ice lens heave increases especially for BF conditions. We explain this difference with TF due to the formation of longitudinal cracks that facilitate water flow (cf. Fig. 6, subsection 5.2) which is exacerbated by the fact that in BF, the water flows downwards aided by gravity.

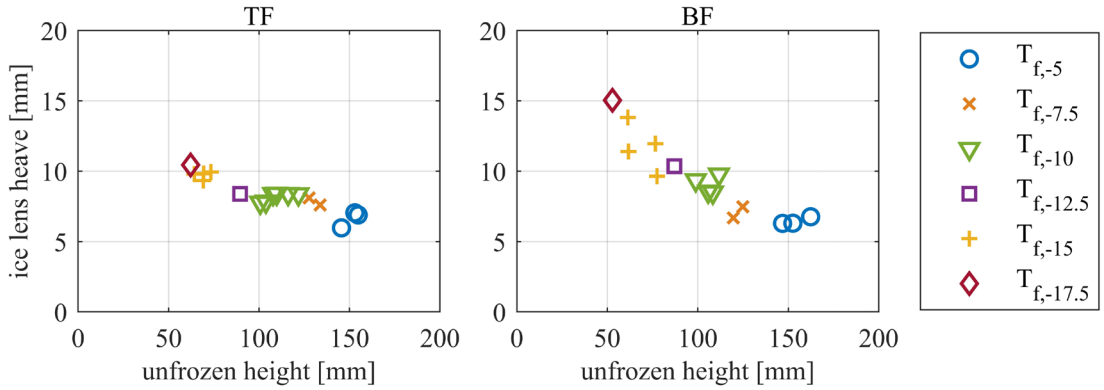

Fig. 11 Ice lens heave for different absolute freezing temperatures (T_f in °C) over the height of the unfrozen part after 150 h from the beginning of the quasi-steady state for TF and BF

The effect of gravitational water inflow decreases with a thicker unfrozen soil part (i.e., warmer freezing temperatures, T_f) because the cracks do not fully penetrate the unfrozen soil, as shown for temperatures of -5°C and -7.5°C. This explains why for these temperatures, both values in Fig. 11 are very similar for BF and TF. In this case the heave difference between BF and TF is primarily caused by the overburden load which changes slightly depending on the position of the frost line.

Concluding, the differences between TF and BF are attributed to the water flow direction, the permeability changes due to cracking and the unfrozen soil height. Independent of the freezing direction, the unfrozen soil height mainly governs the ice lens heave. This can be explained by the hydraulic gradient which increases with decreasing flow path if the hydraulic head and the suction force at the ice lens are the same at each test. This can be assumed because the suction at the ice lens mainly depends on temperature (e.g., Clausius-Clapeyron equation) and, moreover, the same soil was used for all tests, so the segregation temperature should be the same.

6.2 Temperature gradient $gradT_f$

Fig. 12 shows the ice lens heave 150 h after the beginning of the thermal quasi-steady state for temperature gradients of 0.8 °C/cm, 1.0 °C/cm (corresponds to the experiments with T_f = -10°C in section 6.1 due to same freezing depth at thermal quasi-steady state) and 1.5 °C/cm along the frozen area. The corresponding heights of the unfrozen area or flow paths are controlled by the temperature boundary conditions. Despite different temperature gradients in the frozen area, the same frost heave occurs. It can be therefore, concluded that the temperature gradient in the frozen area has no relevant impact on the formation of ice lenses at thermal quasi-steady state in the investigated range. This result corresponds to the findings in section 6.1, where the unfrozen height or flow path mainly influences the ice lens heave.

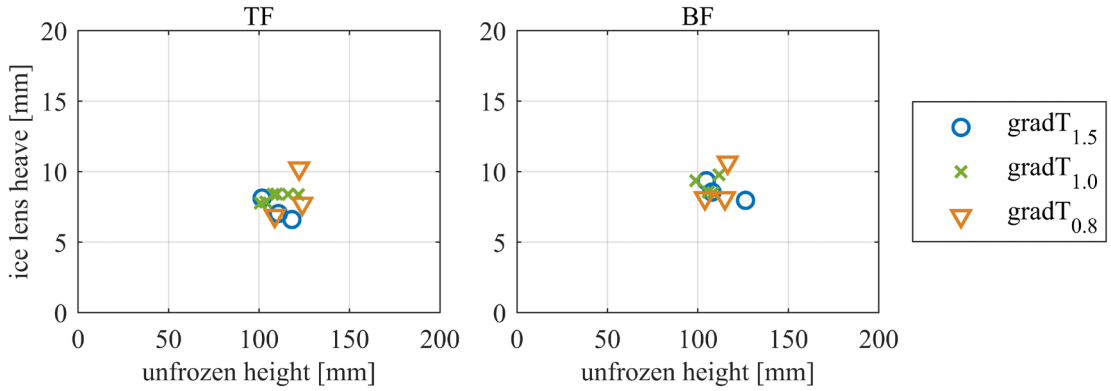

Fig. 12 Ice lens heave for different temperature gradients ($gradT_f$ in °C/cm) along the frozen soil over the height of the unfrozen part after 150 h from the beginning of the quasi-steady state for TF and BF

6.3 External load p

The following tests were carried out by applying a load (p) on the soil sample. Each experiment contains a consolidation and freezing phase. During consolidation phase the soil settles under a defined constant load until the deformation stops. Afterwards the freezing process with a temperature of -12.5°C is initiated and frost heaving starts.

Fig. 13 shows the longitudinal soil strain rate during consolidation for TF and BF calculated as soil deformation over the maximum settlement at the end of consolidation. After approx. 4 days (96 h) of consolidation the freezing

phase was initiated. The measured settlement fluctuates slightly since the automatic load readjustment just took place every 60 seconds. The calculation of settlement difference over a time step produces the oscillating curve. At the beginning of the consolidation phase, the specimen is less stiff which increases this effect. To focus the relevant progress over time the ordinate in Fig. 13 ends at 0.2.

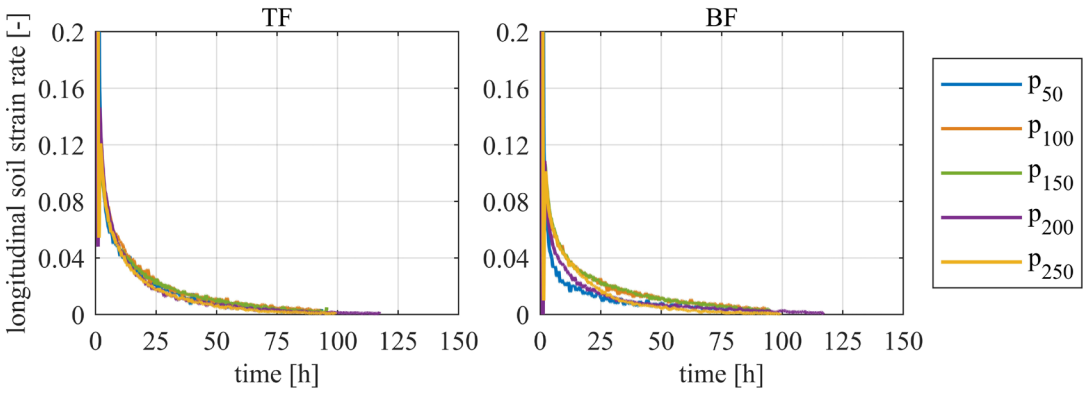

Fig. 13 Longitudinal soil strain during the consolidation phase for different loads (p in kPa) for TF and BF

During the consolidation phase the soil settles and water is expelled out of the sample into the external reservoir. With the beginning of the freezing process the sample starts to expand due to pore water expansion. Further the emerging suction as a result of thermodynamic unbalance causes the water to flow back into the soil sample and heave due to ice lens formation occurs. The frost heave results during thermal transient freezing are given in Fig. 14 and during thermal quasi-steady state in Fig. 15. For both thermal states the results are compared with zero load tests p_0.

The frost heaves during thermal transient freezing (Fig. 14) are related to the height of the frozen part, similar to Fig. 9 (subsection 6.1), to eliminate influences of the freezing depth on frost heave. The lower porosity resulting from the consolidation phase reduces the frost heave due to pore water expansion compared to zero load freezing. With greater load frost heave slightly decreases, although the results show the differences between different applied loads are not dramatic. The deviating curve at a load of 150 kN in BF is attributed to irregularities in the initial temperature. Importantly, the formation of a dominating single ice lens at the end of thermal transient freezing, as experienced at zero load tests (cf. Fig. 9), was not observed. Qualitatively there are no differences between the TF and BF results with load, but quantitatively the heave results of TF exceed BF because of less additional soil weight that has to be overcome.

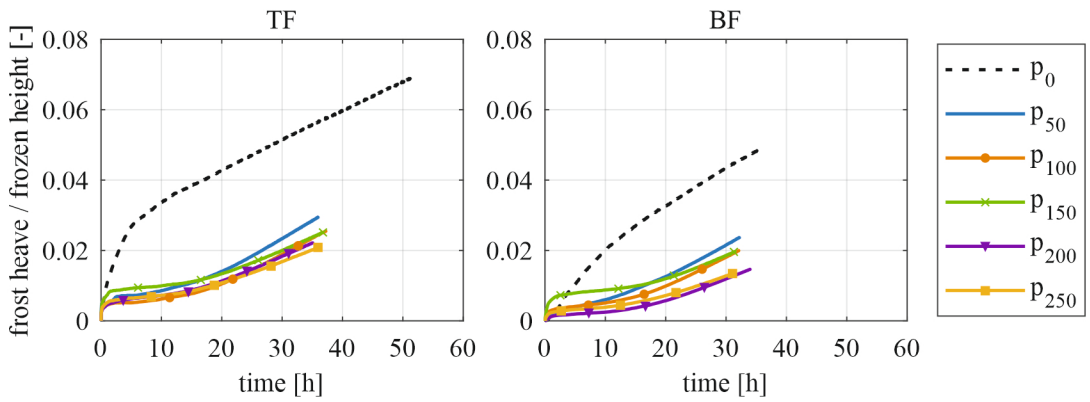

Fig. 14 Frost heave related to the frozen height at the thermal transient state for a freezing temperature of -12.5°C and varied loads (p in kPa) for TF and BF

Fig. 11 and Fig. 12 have shown that the height of the unfrozen area has a great effect on ice lens formation during thermal quasi-steady state. For the examination of ice lens heave during loading, the influence of the unfrozen soil height should be minimized to focus on heave reduction based on the specific load. For this, all tests were carried out with the same freezing temperature of -12.5°C. However, during consolidation at different load magnitudes changes in porosity and water content occur and influence heat conduction. Thus, the unfrozen heights differ despite of same freezing temperatures (Fig. 15, right, and Fig. 16, right).

Fig. 15 and Fig. 16 show the ice lens heave as well as the height of the unfrozen soil at the thermal quasi-steady state for a freezing temperature of -12.5°C and varied loads. Generally, the frost heave increases with lower loading, but the results question the influence of the unfrozen height on heaving. For example, comparing BF (Fig. 16) with a load of 50 and 100 kPa the frost heave results are almost similar, but the unfrozen height or flow path for sucked water at 50 kPa is greater. At BF (Fig. 16), the lowest heave value is reached at 200 kPa instead of 250 kPa which could only be explained if the displacement transducer did not work properly in this test. This is because other measured parameters, such as temperature and surcharge are constant when the curve bends.

Besides the effect of unfrozen soil height, the greater difference at BF (Fig. 16) between unloaded and low loaded test results is attributed to the crack formation which influences the sample permeability in the unfrozen area. As expected, greater loading reduces crack formation (images are provided in the Supplementary Material 3).

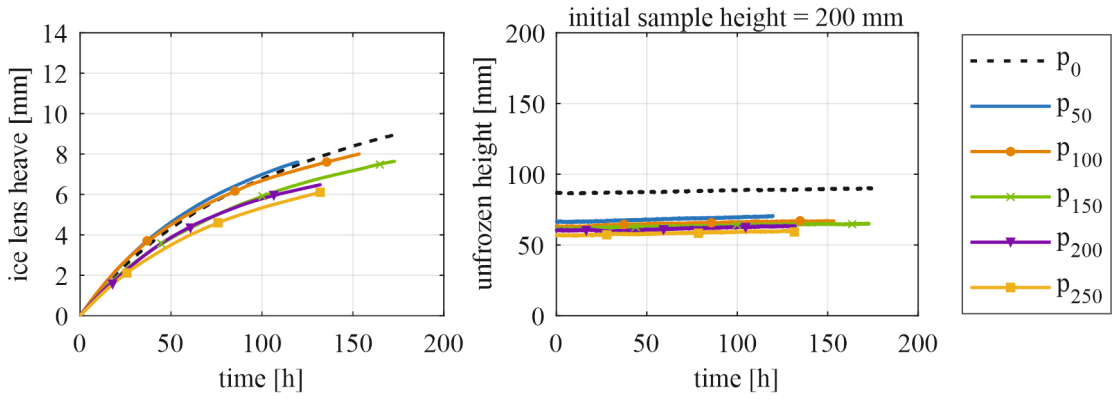

Fig. 15 Ice lens heave (left) and associated unfrozen soil height (right) at the thermal quasi-steady state for a freezing temperature of -12.5°C and varied loads (p in kPa) for TF

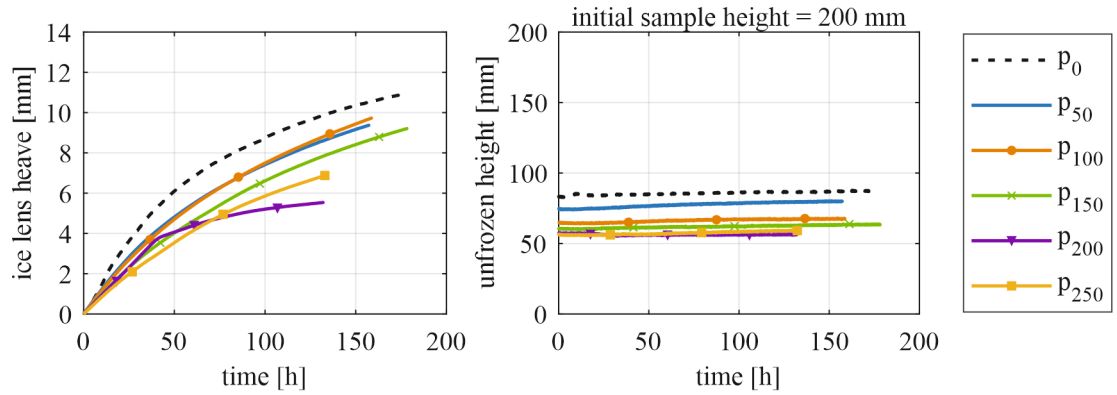

Fig. 16 Ice lens heave (left) and associated unfrozen soil height (right) at the thermal quasi-steady state for a freezing temperature of -12.5°C and varied loads (p in kPa) for BF

Fig. 17 shows, similar to Fig. 11 and Fig. 12, the ice lens heave at quasi-steady state conditions for different unfrozen heights 100 h after reaching the thermal quasi-steady state. Since the consolidation phase takes approx. 4 days the freezing phase was selected to 100 h, as 150 h freezing at thermal quasi-steady state conditions (cf. Fig. 11 and Fig. 12) was not applicable. The black circles indicate the heave results under zero load, carried out in section 6.1.

To investigate the influence of temperature, additional tests using a freezing temperature of -10°C and -5°C are used for the maximum load of 250 kPa. The ice lens heaving decreases with greater load and, at TF (Fig. 17, left), for 250 kPa is almost parallel to zero load results. At BF (Fig. 17, right) loaded frost heave results are not parallel

to the results without loading. It is assumed that the reduced crack formation reduces permeability and therefore the growth of the ice lens. With higher loading TF and BF heaving results are more consistent which emphasize the assumption that the crack-induced increasing permeability and better water accumulation due to gravitational effects at BF is reduced by surcharge.

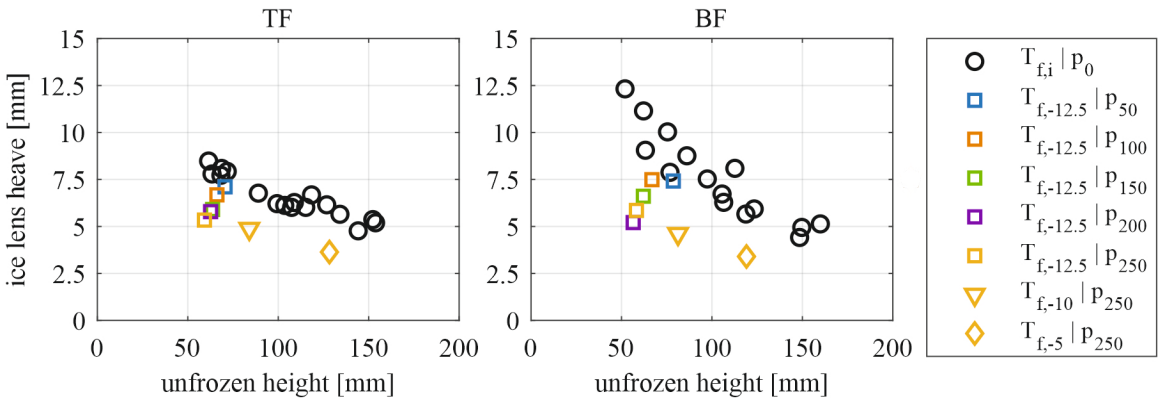

Fig. 17 Ice lens heave at different temperatures (T_f in °C) and loads (p in kPa) over the height of the unfrozen part after 100 h from the beginning of the quasi-steady state for TF and BF

The results show that besides loading, the influence of the unfrozen soil height or the flow path of sucked water, respectively, is present. The TF and BF results differ as long as the crack formation in the unfrozen area has an effect on the permeability. The greater the magnitude of loading the more crack opening is impeded by confining pressure and the minor heave differences between TF and BF.

7 Conclusion

The method of AGF is common for inner-city tunnelling construction projects. Since ice lenses form especially in frost susceptible soils, strong deformations occur, which magnitude depends on the boundary conditions. In this work the influence of different freezing directions, TF vs. BF, on frost heaving is investigated considering the special thermal and load boundary conditions of an AGF. Therefore, 62 frost heave tests were carried out in a novel test device with testing periods up to 10 days, providing a comprehensive database of ice lens formation during the thermal steady state. This state simulates the holding phase of an AGF, where cooling only maintains the thickness of the frozen body and no further frost penetration occurs.

During the thermal transient phase which is characterized by a growing frost body with moving frost line, there was only a negligible ice lens formation observed which is due to fast frost penetration. The process is dominated by the magnitude of the boundary cold temperatures only. Frost heaving during TF is usually larger than BF heave which is attributed to greater soil weight and consolidation effects in the BF conditions.

At thermal-steady state one relevant factor with great impact on the magnitude of frost heaving is the height of the unfrozen soil, which can also be seen as proxy for the water flow path. This is directly a function of temperature at the boundary conditions where lower temperatures reduce the unfrozen part (i.e., the colder it is the boundary, the smaller the unfrozen region of the soil). A shorter unfrozen part increases the hydraulic gradient for the same boundary hydraulic conditions and, thus, the water flow velocity to the ice lens. This effect is observed independently of the freezing direction.

Conversely to the transient stage, BF exhibits larger frost heave than TF conditions for almost all conditions. This is due to the formation of longitudinal cracks along the unfrozen zone that initiate during ice lens formation and are caused by suction. The cracks emerge when water at the warm side of the ice lens is drained off for ice lens growth. These cracks favour water flow towards the ice lens, hence, increasing the ice lens size. The closer the ice lens to the water reservoir, the greater is the effect of an improved water accumulation at the growing ice lens. The greatest frost heave occurs when the unfrozen part is short, and cracks reach the unfrozen surface. Equivalent hydraulic conditions can naturally occur in real applications when AGF is used within an aquifer. The application of vertical load reduces crack formation and therefore, for this cases, BF and TF present similar heave magnitudes. In the case of our tests, an applied load of 150 kPa seemed to be the threshold from which the cracks would not form.

The relationship between the unfrozen soil height and the ice lens heave is not linear and different for BF and TF freezing. This is of interest for long-term soil freezing and will be analyzed in detail in future research work.

8 **Acknowledgements**

This work was supported by the German Research Foundation (DFG) under the project “Investigation and calculation of frost heave considering specific boundary conditions of ground freezing", grant number 409760547. The funding is herewith gratefully acknowledged.

References

1. Staender, W., *Das Gefrierverfahren im Schacht-, Grund-und Tunnelbau*, in *Die Anwendung der Kälte in der Verfahrens-und Klimatechnik, Biologie und Medizin*. 1967, Springer. p. 173-227.
2. Hartge, K.H., *Einführung in die Bodenphysik*. 1978, Stuttgart: Ferdinand Enke Verlag.
3. Martin, R.T., *Rhythmic ice banding in soil.* Highway Research Board Bulletin, 1959(218).
4. Kaplar, C.W., *Phenomenon and mechanism of frost heaving.* Highway Research Record, 1970. **304**: p. 1-13.
5. Sheng, D., K. Axelsson, and S. Knutsson, *Frost Heave due to Ice Lens Formation in Freezing Soils: 1. Theory and Verification.* Hydrology Research, 1995. **26(2)**: p. 125-146.
6. Rempel, A.W., *Frost heave.* Journal of Glaciology, 2010. **56**(200): p. 1122-1128.
7. Ladanyi, B. and O. Andersland, *Frozen ground engineering*. 2004: Wiley.
8. Konrad, J.-M. and N.R. Morgenstern, *Mechanistic theory of ice lens formation in fine-grained soils.* Canadian Geotechnical Journal, 1980. **17**(4): p. 473-486.
9. Auld, F.A., J. Belt, and D. Allenby, *Application of artificial ground freezing.* Proceedings of the XVI ECSMGE, 2015: p. 6.
10. Johansson, T., *Artificial Ground Freezingin Clayey Soils: Laboratory and Field Studies of Deformations During Thawing at the Bothnia Line*. 2009, KTH.
11. Kaplar, C.W., *Freezing test for evaluating relative frost susceptibility of various soils*. 1974: US Army Cold Regions Research and Engineering Laboratory.
12. Penner, E. and T. Ueda, *The dependence of frost heaving on load application - preliminary results.* Proceedings of the International Symposium on Frost Action in Soil, Luleå, Sweden, 1977. **1**: p. 92-101.
13. Loch, J.P.G. and B.D. Kay, *Water redistribution in partially frozen, saturated silt under several temperature gradients and overburden loads.* Soil Science Society of America Journal, 1978. **42**: p. 400-406.

14. Jin, H.W., Lee, J., Ryu, B.H., and Akagawa, S., *Simple frost heave testing method using a temperature-controllable cell.* Cold Regions Science and Technology, 2019. **157**: p. 119-132.

15. Konrad, J.-M. and N.R. Morgenstern, *The segregation potential of a freezing soil.* Canadian Geotechnical Journal, 1981. **18**(4): p. 482-491.

16. Konrad, J.-M. and N.R. Morgenstern, *Prediction of frost heave in the laboratory during transient freezing.* Canadian Geotechnical Journal, 1982. **19**(3): p. 250-259.

17. Loch, J.P.G., *Thermodynamic equilibrium between ice and water in porous media.* Soil Science, 1978. **126**(2): p. 77-80.

18. Sweidan, A., Niggemann, K., Heider, Y., Ziegler, M., and Markert, B., *Experimental study and numerical modeling of the thermo-hydro-mechanical processes in soil freezing with different frost penetration directions.* Acta Geotechnica, 2022. **17**(1): p. 231-255.

19. Xia, D., Arenson, L.U., Biggar, K.W., and Sego, D.C., *Freezing process in Devon silt-using time-lapse photography*. In *58th Canadian Geotechnical Conference, Saskatoon, Saskatchewan*. 2005.

20. Mackay, J.R., *Ice-wedge cracks, Garry Island, Northwest Territories.* Canadian Journal of Earth Sciences, 1974. **11**(10): p. 1366-1383.

21. Chamberlain, E.J. and A.J. Gow, *Effect of freezing and thawing on the permeability and structure of soils.* Engineering Geology, 1979. **13**(1-4): p. 73-92.

22. Arenson, L., D. Sego, and W.A. Take. *Measurement of ice lens growth and soil consolidation during frost penetration using particle image velocimetry (PIV)*. in *60th Canadian Geotechnical Conference & 8th Joint CGS/IAH-CNC Groundwater Conference*. 2007. Ottawa, Ontario, Canada.

23. Arenson, L.U., Azmatch, T.F., Sego, D.C, and Biggar, K.W., *A new hypothesis on ice lens formation in frost-susceptible soils*. in *Ninth International Conference on Permafrost, Fairbanks, Alaska*. 2008. **1**: p. 59-64.

24. Niggemann, K. *Investigation of frost heave considering the boundary conditions of artificial ground freezing*. in *Transportation Soil Engineering in Cold Regions*. 2020. St. Petersburg, Russia: Springer, Singapore.

25. Yin, Q., Andò, E., Viggiani, G., and Sun, W., *Freezing-induced stiffness and strength anisotropy in freezing clayey soil: Theory, numerical modeling, and experimental validation.* International Journal for Numerical and Analytical Methods in Geomechanics, 2022. **46**(11): p. 2087-2114.